Atmósfera 22(1), 1-31 (2009)

Mexican drought: an observational modeling and tree ring study of variability and climate change

R. SEAGER, M. TING
Lamont-Doherty Earth Observatory of Columbia University, Palisades, NY 10964, USA
Corresponding author: R. Seager; e-mail: seager@ldeo.columbia.edu

M. DAVIS
Department of History, University of California at Irvine, CA, USA

M. CANE, N. NAIK, J. NAKAMURA, C. LI, E. COOK
Lamont-Doherty Earth Observatory of Columbia University, Palisades, NY 10964, USA

D. W. STAHLE
Tree Ring Laboratory, University of Arkansas, Fayetteville, Arkansas, USA

Received February 22, 2008; accepted July 28, 2008

RESUMEN

Se examina la variabilidad del hidroclima mexicano –con un enfoque particular en las sequías persistentes– mediante observaciones, modelos de simulación forzados por las temperaturas históricas de la superficie marina (SST por sus siglas en inglés), reconstrucciones paleoclimáticas basadas en anillos de árboles, modelos de simulación y proyecciones de cambios de clima tanto de origen natural como antrópico. Durante la mitad invernal del año, el hidroclima a lo largo y ancho de México se ve influenciado por la condición del Océano Pacífico tropical, mientras que la influencia del Atlántico es mínima. Cuando las condiciones de El Niño emergen, los inviernos mexicanos tienden a ser mas húmedos. En la mitad veraniega, cuando El Niño prevalece, el norte de México es también más húmedo, mientras que el sur es más seco. Cuando el Atlántico norte tropical se calienta, el norte de México se caracteriza por ser más seco y el sur más húmedo. Estas relaciones son bien reproducidas en los conjuntos de modelos de simulación de la atmósfera, forzados por las SST históricas para el período que se extiende de 1856 a 2002. Se utilizan ensambles extensos de integraciones de 100 días para examinar día con día la evolución de la circulación atmosférica y la precipitación en respuesta a la repentina imposición de la anomalía de la SST de El Niño en la mitad veraniega del año. Las ondas de Kelvin se propagan hacia el este y causan de inmediato una divergencia incrementada de la columna integrada de humedad y precipitación reducida sobre los mares americanos tropicales y mares intra-americanos. En un lapso de pocos días se desarrolla una anomalía de alta presión sobre el Golfo de México. Un modelo forzado no lineal demuestra que esa anomalía se origina debido una reducción en el calentamiento de la atmósfera sobre los mares tropicales intra-americanos del Atlántico. Para verificar simulaciones de modelos forzados por SST históricas se usan reconstrucciones a partir de anillos de árboles que se extendien a épocas anteriores a los registros instrumentales de precipitación. La sequía de la primera mitad de la década de 1950 en el norte de México parece ser la más severa desde mediados del siglo XIX y probablemente ocurrió en respuesta tanto a los efectos multianuales de La Niña como a un Atlántico tropical cálido. La sequía de la década de 1890 también fue severa y aparenta ser el resultado único de una Niña multianual. La sequía que inició en la década de 1990 no sobrepasa esas sequías tanto en duración como en severidad. Datos obtenidos mediante estudios de anillos de áboles que se extienden hasta el siglo XIV sugieren que a finales del siglo XVI hubo una sequía prolongada (megasequía) que pudo haber sido la más larga en la historia de México. Aunque durante la última década, el norte y centro de México han sido más secos que las décadas anteriores, el patrón continental de cambio hidroclimático asociado, no

corresponde con lo que los modelos proyectan que debería ocurrir a consecuencia de un aumento del efecto invernadero y del calentamiento global. Sin embargo, los modelos pronostican robustamente que México será más árido a consecuencia del calentamiento global y que la sequía ya debería haber iniciado. Por el momento, es probable que en la naturaleza este proceso se vea enmascarado por la variabilidad natural del océano y de la atmósfera.

ABSTRACT

Variability of Mexican hydroclimate, with special attention to persistent drought, is examined using observations, model simulations forced by historical sea surface temperature (SST), tree ring reconstructions of past climate and model simulations and projections of naturally and anthropogenically forced climate change. During the winter half year, hydroclimate across México is influenced by the state of the tropical Pacific Ocean with the Atlantic playing little role. Mexican winters tend to be wetter during El Niño conditions. In the summer half year northern México is also wetter when El Niño conditions prevail, but southern México is drier. A warm tropical North Atlantic Ocean makes northern México dry and southern México wet. These relationships are reasonably well reproduced in ensembles of atmosphere model simulations forced by historical SST for the period from 1856 to 2002. Large ensembles of 100 day long integrations are used to examine the day to day evolution of the atmospheric circulation and precipitation in response to a sudden imposition of a El Niño SST anomaly in the summer half year. Kelvin waves propagate east and immediately cause increased column-integrated moisture divergence and reduced precipitation over the tropical Americas and Intra-America Seas. Within a few days a low level high pressure anomaly develops over the Gulf of México. A forced nonlinear model is used to demonstrate that this low is forced by the reduced atmospheric heating over the tropical Atlantic-Intra-America Seas area. Tree ring reconstructions that extend back before the period of instrumental precipitation data coverage are used to verify long model simulations forced by historical SST. The early to mid 1950s drought in northern México appears to have been the most severe since the mid nineteenth century and likely arose as a response to both a multiyear La Niña and a warm tropical North Atlantic. A drought in the 1890s was also severe and appears driven by a multiyear La Niña alone. The drought that began in the 1990s does not exceed these droughts in either duration or severity. Tree ring records extending back to the fourteenth century suggest that the late sixteenth century megadrought may have been the longest drought to have ever affected México. While the last decade or so in north and central México has been drier than preceding decades, the associated continental pattern of hydroclimate change does not fit that which models project to occur as a consequence of rising greenhouse gases and global warming. However, models robustly predict that México will dry as a consequence of global warming and that this drying should already be underway. At least for now, in nature, this is likely obscured by strong natural atmosphere-ocean variability.

Keywords: Mexican drought, climate variability, El Niño, hydroclimate change.

1. Introduction

The causes of persistent droughts in North America have become clearer in recent years largely as a result of analysis of simulations with models forced by historical sea surface temperatures (SST). This work has demonstrated that multiyear droughts over the Great Plains and southwestern North America have been forced by equally persistent anomalous SST with cold, La Niña-like, SST in the Pacific playing the dominant role and warm subtropical North Atlantic SST also sometimes playing a role, as during the 1930s and 1950s droughts (Schubert *et al.*, 2004a; Schubert *et al.*, 2004b; Seager *et al.*, 2005b; Herweijer *et al.*, 2006; Cook *et al.*, 2007; Seager 2007). Newly developed tree ring analyses have also allowed a detailed examination of the Medieval period of heightened aridity in western North America (Cook *et al.*, 2004, 2007; Herweijer *et al.*, 2007; Stahle *et al.*, 2007) and, as for modern droughts, changes in tropical SST have been invoked as the cause, although it is not yet clear what could have caused them (Mann *et al.*, 2005; Herweijer *et al.*, 2006; Graham *et al.*, 2007; Emile-Geay *et al.*, 2007; Seager *et al.*, 2007a; Seager *et al.,* 2007b). Finally Seager *et al*. (2008b), have shown that projections of anthropogenically-forced climate change robustly predict that southwestern

North America is in transition to a more arid climate as part of a general aridification and poleward expansion of the subtropical dry zones (Held and Soden, 2006; Lu *et al.*, 2007).

These advances in our knowledge of past and future North American hydroclimate have tended to focus on climate within the current borders of the United States. However it is clear from Seager *et al.* (2007b) that all of México is projected to become drier in this century with this transition potentially already underway. Indeed, México has experienced a severe, if not unprecedented, drought that began in the mid 1990s and at least continued through the first few years of the current century (when available station data in most data sets ends) (Hallack-Alegría and Watkins, 2007). However, identification of an anthropogenic impact on precipitation in México is complicated by strong internanual and decadal variability of precipitation in the region. The El Niño-Southern Oscillation (ENSO) influences precipitation over all of México during winter, with El Niño bringing wet conditions, as part of a continental scale pattern that also influences the United States (Ropelewski and Halpert, 1986, 1987, 1989, 1996; Seager *et al.*, 2005a). However, unlike the case for almost all of the United States, the sign of the ENSO-forced precipitation signal changes seasonally in the southern parts of México and El Niño brings drying during summer (Englehart and Douglas, 2002). Both summer and winter precipitation are important for México because over half of Mexican agriculture relies on rain in the summer growing season (Conde *et al.*, 2006).

If the model projections are correct, México faces a future of declining water resources that will have serious consequences for public water supply, agriculture and economic development. Assessing whether anthropogenic change is yet evident requires a better understanding of the mechanisms of Mexican precipitation variability and change, and that is what we attempt here. Drought is more complex than a reduction in precipitation alone and can be strongly influenced by variations in temperature that influence evaporative demand, but all droughts do involve a reduction of precipitation. Here we will focus on the nature and causes of precipitation variations across México looking at both the winter and summer half years. This will be done using observations, ensembles of model simulations forced by historical SST, tree ring reconstructions of hydroclimate back to the fourteenth century, model simulations forced by idealized SST anomalies and simulations and projections of anthropogenic climate change.

2. Data and models

The gridded precipitation and temperature data used here comes from the Universidad Nacional Autónoma de México (UNAM), which covers 1901 to 2002. Unlike the data sets of the Global Historical Climatology Network or the Climate Research Unit (CRU) of the University of East Anglia (Mitchell and Jones, 2005), the UNAM data retains better coverage across México after the mid 1980s. The station coverage is very sparse in the early part of the twentieth century and we restrict our analysis to the period from 1945 on. The UNAM data is available from the International Research Institute for Climate and Society (http://ingrid.ldeo.columbia.edu/SOURCES/UNAM/gridded/monthly/v0705/). We also use the outgoing long wave radiation precipitation index (OPI) from the satellite only data of the Climate Anomaly Monitoring System (CAMS), which covers from 1979 to November 2007 (Janowiak and Xie, 1999). Sea surface temperature data comes from the HadISST data set (Rayner *et al.*, 2003) from 1870 on and from Kaplan *et al.* (1998) to extend the data back to 1856. Tree ring reconstructions of summer Palmer Drought Severity Index (PDSI) are taken from an updated version of the North American Drought Atlas (NADA) as described in Cook *et al.* (2004; 2007). The updated NADA (called NADA v2a) increases the number of tree ring records in North America to 1825 from 835 in the original NADA. Tree records are extended to

the present with instrumental PDSI from Dai *et al.* (2004) after some further application of quality control to remove extreme values from the instrumental PDSI.

The atmosphere model is the National Center for Atmospheric Research Community Climate Model 3 (CCM3) (Kiehl *et al.*, 1998) and has been used in our prior studies of North American drought. Here we use the model in four configurations with details provided in Seager *et al.* (2005b).

1. POGA (Pacific Ocean-Global Atmosphere): In this case historical tropical Pacific SST are specified (20° S-20° N) and climatological SST are imposed elsewhere. Between 20 and 30° of latitude in the Pacific the atmosphere model sees an SST that is a weighted combination of the observed historical SST and the climatological SST at that point with the weighting favoring the climatological SST with increasing latitude.
2. POGA-ML (POGA-Mixed Layer): This has the same tropical Pacific historical SST forcing as POGA but has a mixed layer ocean outside of the tropical Pacific Ocean that computes SST anomalies using the anomalous surface heat fluxes.
3. TAGA (Tropical Atlantic-GA Historical Tropical Atlantic SST are imposed between 30° N and 30° S, and climatological SST are used elsewhere.
4. GOGA (Global Ocean-GA): In this case historical observed SST are specified globally.

The SST data used comes from two sources of ship and satellite observations. The SST data of Kaplan *et al.* (1998) are used for the tropical Pacific for the entire period from January 1856 to August 2007. Elsewhere the HadISST data are used. Since the HadISST data begins in 1870, for the GOGA simulations during the period from 1856 to 1870, and outside the tropical Pacific, Kaplan data is used where available and HadISST climatological values where not. Sea ice is held at climatological values given by HadISST. Each ensemble has 16 members (except TAGA which has 8) begun using different atmospheric initial conditions on January 1, 1856 and the simulations run through August 2007. Here we primarily examine the ensemble mean, which emphasizes the variability forced by the imposed SST (either tropical Pacific or global) that is common to all ensemble members, while the weather 'noise' is uncorrelated between ensemble members and largely disappears after averaging across the ensemble.

Modeled and projected climate change is assessed using data from the Intergovernmental Panel on Climate Change Assessment Report Four (IPCC AR4). We obtained data from 24 coupled models and first computed a model mean if for a given model there was more than one ensemble member. Then the data were averaged together using all the models to create a multimodel ensemble mean. Here the ensemble mean isolates the climate change due to changes in the specified radiative forcing, which is the same in all the models. Data from the simulations with known and estimated changes in radiative forcing between 1900 and 1999, together with data from the projections of climate beyond 2000 using the SRA1B emissions scenario, were used.

3. Observed relationships between Mexican precipitation and tropical SST

The links between tropical SST and Mexican precipitation can usefully be determined through a multiple regression analysis using indices of tropical Pacific and tropical North Atlantic SST. The tropical Pacific (TP) index is the SST anomaly averaged over the region of ENSO activity between 5° S and 5° N and 180° W and 90° W, and the tropical North Atlantic (TNA) index describes SST variations in the northern subtropical Atlantic between the equator and 30° N. Multiple regression

was chosen to determine the impacts of the TP acting alone and the tropical Atlantic acting alone and, within the Pacific pattern, includes any impact on precipitation that comes from Atlantic SST variations that are forced by the tropical Pacific. The analysis was performed using the UNAM precipitation data from 1945 to 2002, separating into winter (November through April) and summer (May through October) half years. The analysis was undertaken on data that was not time filtered but the patterns are the same when a 6 year low pass filter is applied to emphasize multiyear variations (not shown). The regression coefficients are shown here using both contours and colors. The coloring is applied only where the correlation is significant at the 5% level.

Results for the winter half year are shown in Figure 1. During an El Niño winter half year there is an increase in precipitation across most of the United States (except the northwest Pacific) and also across almost all of México and the Caribbean islands. The splitting of this pattern into maxima on either coast of México is probably influenced by the intervening topography of the Sierra Madre Occidental and Sierra Madre Oriental. This pattern is generally statistically significant including over northern México. During the winter half year a warm subtropical North Atlantic causes dry conditions in a region that includes northern México and parts of the central and southwestern U.S. although with marginal statistical significance.

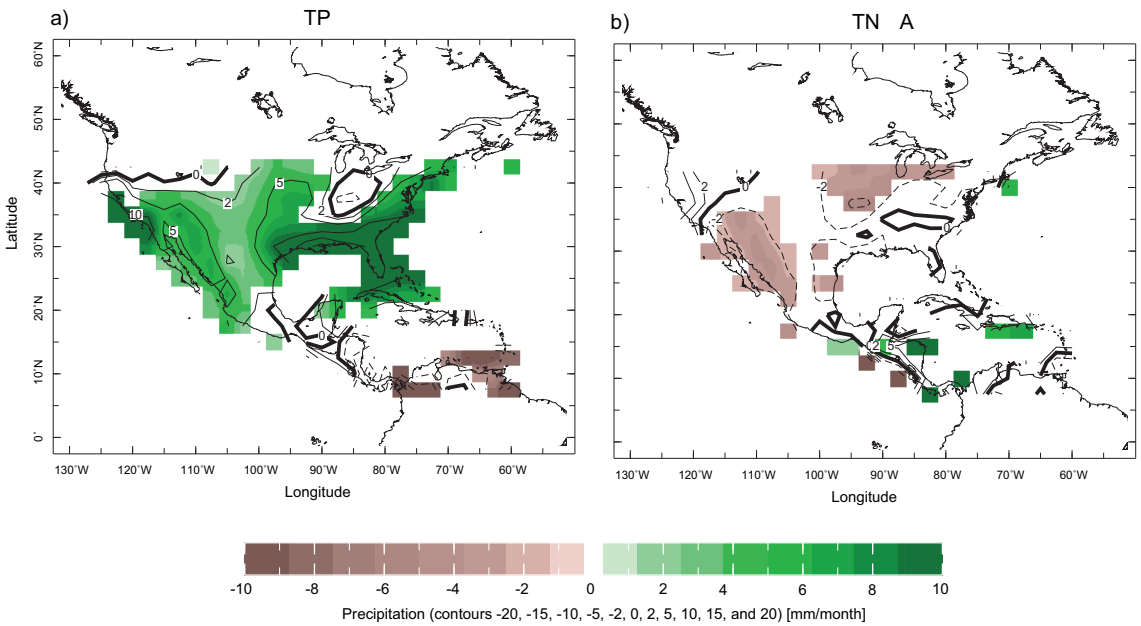

Fig. 1. The multiple regression between precipitation and the tropical Pacific (TP, left) and tropical North Atlantic (TNA, right) SST indices (see text for definition) for the November through April half year using the UNAM precipitation data set and for 1945 to 2002. The regression coefficient in mm/month per standard deviation of the SST index is both contoured and colored but coloring is applied only where the relationship is signifcant at the 5% level.

During the summer half year (Fig. 2) El Niño conditions also bring increased precipitation to the U. S. southwest and northwestern México although with less statistical significance than in winter. However, unlike in winter, El Niño in summer causes southern México to be dry as part of a general drying of Central America and northern South America. (In the annual mean the summer

season signal dominates for southern México meaning that, for example, multiyear Las Niñas, will tend to be wet). In this part of the year warm subtropical North Atlantic SST anomalies are associated with dry in northern México and wet in southern México, central America and the Caribbean islands, although the relations are not statistically significant for most of México.

These regression maps were also computed using the CRU data. Since coverage over México is poor after the mid 1980s in the CRU data, we examined the 1930 to 1985 time period. The same patterns of relationships between precipitation and the TP and TNA indices were reproduced using the CRU data, but with somewhat greater statistical significance (not shown).

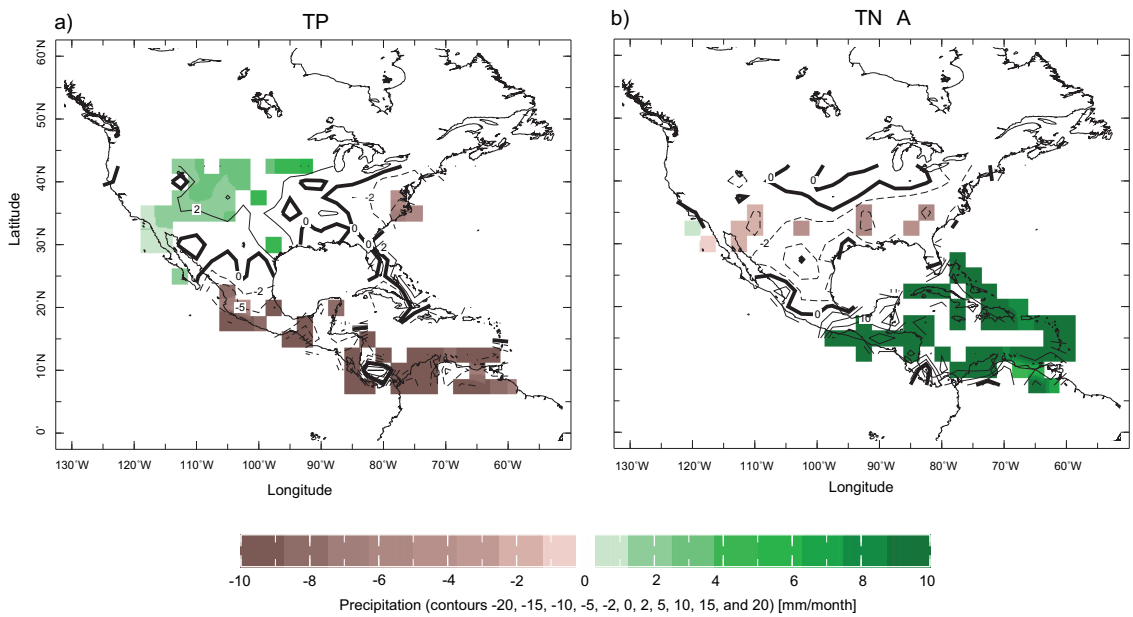

Fig. 2. Same as Fig. 1 but for the May through October half year.

4. Modeled relationships between Mexican precipitation and tropical SST

To check the robustness and causality of the observed relationships between precipitation over México and SST in the Pacific and Atlantic oceans, we also performed single regressions using the ensemble mean of the POGA and TAGA simulations which are forced solely by Pacific or Atlantic SST variations, respectively. Results for the winter half year are shown in Figure 3. Pacific forcing alone provides a very zonally symmetric response (within this domain) with wet conditions during El Niño events across the United States (except for the Pacific northwest) and México, and dry conditions further south in the Americas. This pattern is clearly very similar to the observed pattern, except that it misses the presumed effect of Mexican topography (which is not suprising given the coarse resolution of the model). Warm Atlantic forcing in winter creates dry conditions in the United States and most of México apart from the Yucatán peninsula. This is again notably similar to observations, but the signal is clearer presumably because the model ensemble mean isolates the SST forced component more clearly than occurs in nature. However the modeled relationship to Atlantic SST also appears to be stronger than that observed.

The modeled response to Pacific forcing during the summer half year (Fig. 4) is clearly different than in winter. Precipitation anomalies during El Niño are no longer zonally oriented and wet

conditions are limited to the United States and northeastern México, while dry conditions occupy a wedge shaped feature that covers the entire Caribbean and Gulf of México, Florida, southern México, Central America and northern South America. This pattern appears similar to that observed. Warm tropical North Atlantic forcing in the summer half year dries the United States except in the Southeast, dries northwest México and makes southern México wet along with the Caribbean and Gulf of México and northern South America, a pattern that is again very similar to that observed but stronger.

These analyses make clear that precipitation variability over México is controlled by both the tropical Pacific Ocean and the tropical Atlantic Ocean. During the winter half year El Niño makes the whole of México wet, while during the summer half year it makes northern México wet and southern México dry. These relationships are adequately reproduced in the climate model simulations forced by historical SST. The same relationships can be derived by beginning with indices of precipitation over México and regressing SST onto those indices (not shown) indicating the robustness of these relationships. The Atlantic influence is clearer and stronger in the model than in observations.

It should be noted that in coastal México a significant proportion (up to a quarter on the Pacific coast, Matt Barlow, pers. comm., 2008) comes from tropical cyclones and variations of this will be reflected in the observed analysis to the extent that it correlates with the tropical SST indices. However, the tropical cyclone associated precipitation variability will not be captured in the large scale model simulations used here and this may account for some of the discrepancies between observed and modeled precipitation during the summer half year.

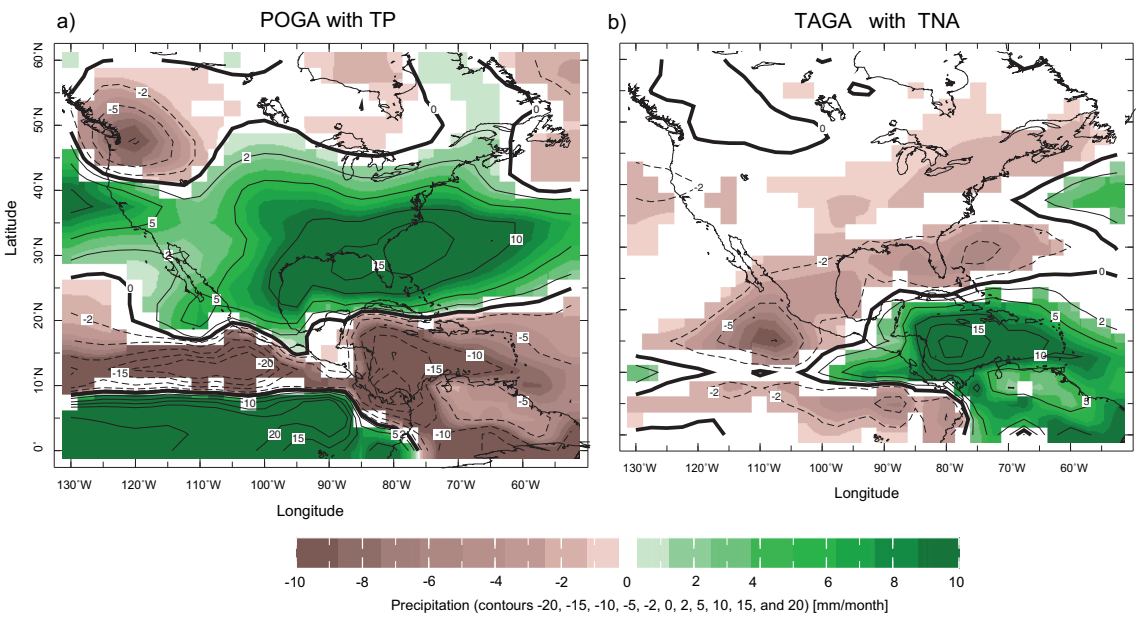

Fig. 3. The regression of modeled precipitation on the tropical Pacific SST index with tropical Pacific SST forcing alone (POGA, left) and on the tropical Atlantic SST index with tropical Atlantic SST forcing alone (TAGA, right) for the November through April half year and the 1945 to 2002 period.

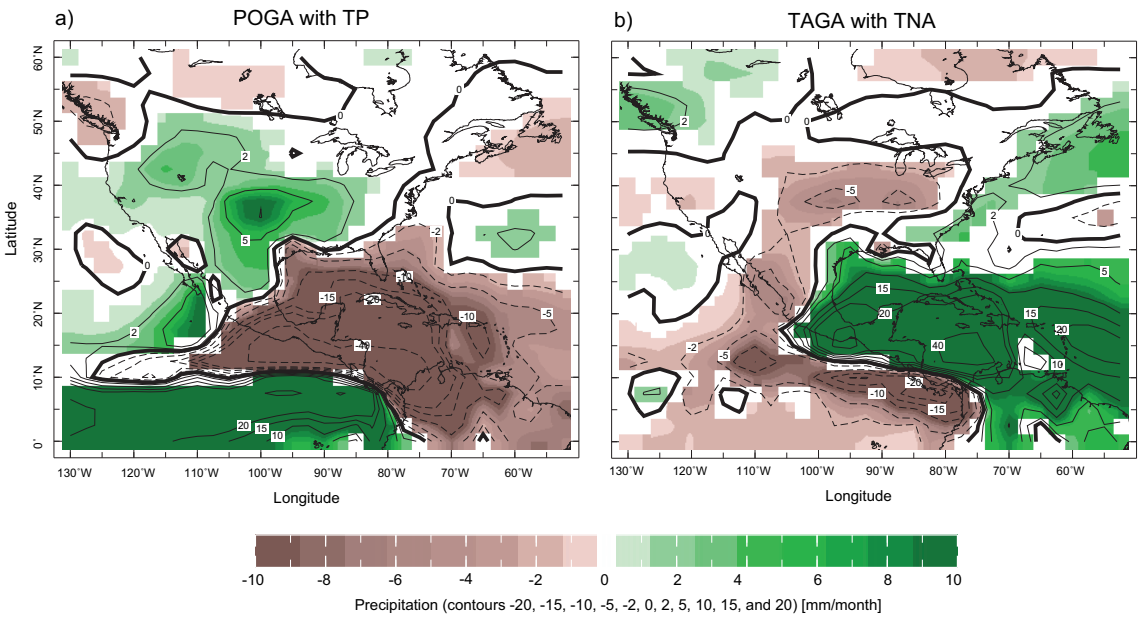

Fig. 4. Same as Fig. 3 but for the October through May half years of the 1945 to 2002 period.

5. Modeled and observed history of Mexican drought since 1945

The comparison of the spatial pattern of observed and modeled precipitation anomalies over the México, Central America and tropical Atlantic region described earlier suggests that the observed SST-forced model simulations should be able to simulate aspects of the observed history of precipitation over México. To examine this we compare time series of observed and modeled precipitation averaged over chosen regions.

During the winter half year the patterns of tropical Pacific and Atlantic forced precipitation variations create anomalies of the same sign across México. Hence we created time series of precipitation, for both UNAM observations and the model simulations, averaged over all land areas between 15 and 30° N and 115 and 85° W for the 1945 to 2002 period. A three year low pass filter is applied to emphasize interannual to longer timescale variations. Results are shown using the GOGA, POGA and TAGA simulations in Figure 5, where the shading around the model ensemble means encloses the two standard deviation spread of the model ensembles. Correlation coefficients between all the modeled and observed (or reconstructed) hydroclimate time series shown here are presented in Table I together with those from other model runs not explicitly discussed here.

The modeled precipitation with global SST forcing captures the observed variations quite well during the winter half year, including the drought during the early to mid 1950s, the very wet early 1990s and the subsequent return to a drier winter climate. It is clear that most of these modeled variations are forced by tropical Pacific SST variations (Fig. 5, middle panel), while the tropical Atlantic influence is negligible (Fig. 5, bottom panel). Correlation coefficients between observed and modeled time series for these simulations, and others presented below, are shown in Table I.

The summer half year is more complicated because both the patterns of Pacific and Atlantic forced precipitation variations are of opposite sign in northern and southern México (Figs. 1 through 4).

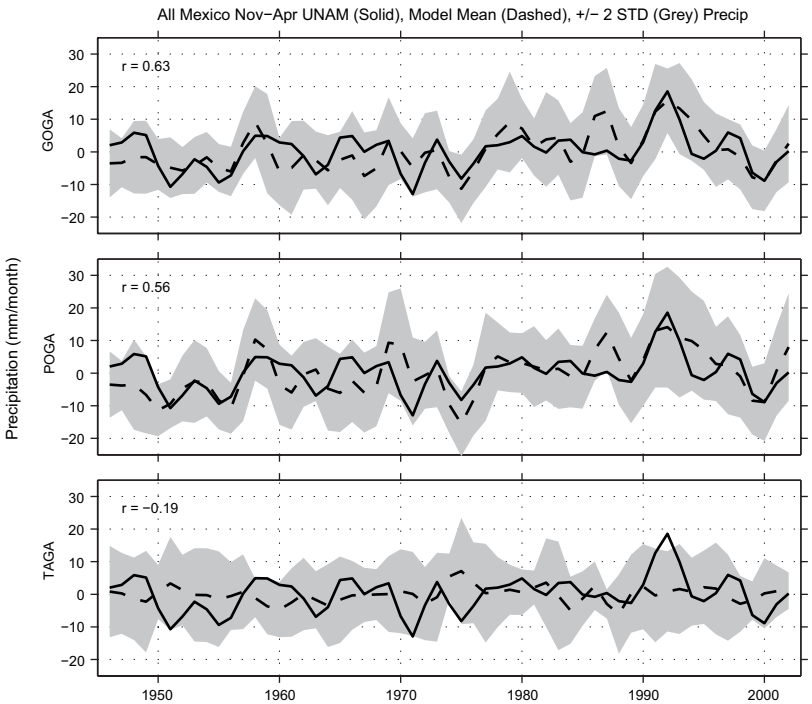

Fig. 5. The observed (sold line) and modeled (dashed lines) precipitation averaged over all of México (land areas between 15 and 30° N and 125 and 85° W) for the November through April half year and for the case with global SST forcing (GOGA, top), tropical Pacific SST forcing alone (POGA, middle) and tropical Atlantic SST forcing alone (TAGA, bottom). The shading is the two standard deviation spread of the model ensemble. All data has been smoothed with a 3 year low pass filter to emphasize interannual and longer timescales. Units are mm per month.

Hence we create precipitation indices for northern México (all land areas between 20 and 30° N and 115 and 95° W) and for southern México (all land areas between 15 and 20° N and 105 and 85° W).

For the southern México area (Fig. 6) the model simulations are clearly less skillful than for winter although aspects of the post 1970 interannual variability are reproduced. However, the

Table I. Correlations coeficients between observed and modeled regionally averaged hydroclimate time series

	All México	N. México		S. México
	1945-2002 Nov-Apr	1945-2002 May-Oct	1856-2005 annual	1945-2002 May-Oct
GOGA	0.63	0.29	0.48	0.29
POGA	0.56	0.21	0.37	0.06
TAGA	-0.19	0.19	-0.02	0.40
POGA-ML	0.66	0.06	0.48	0.24

GOGA model simulates a very wet series of summers around 1960 that did not occur in the UNAM data (nor in the UEA data, not shown) and it also simulated a dry period in the early to mid 1990s that did not occur. Unlike the winter half year, the Atlantic SST forcing plays an important role in summer and the tropical Atlantic SST only-forced model (TAGA) actually does a credible job of simulating aspects of the record.

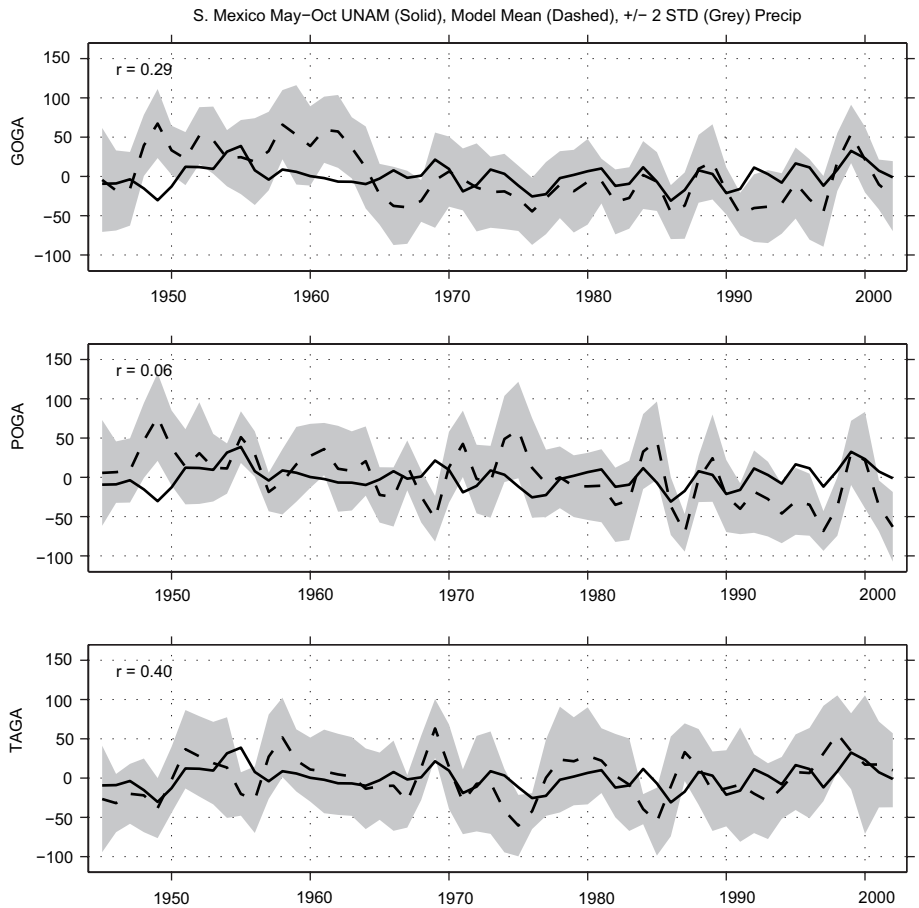

Fig. 6. Same as Fig. 5 but for the summer half year of the southern México region (all land areas in between 15 and 29° N and 110 and 85° W) and for the May through October half year.

Figure 7 shows the corresponding figure for the northern México region. Note that the vertical axis in this figure is different to that for southern México reflecting the fact that summer precipitation variations are much smaller in the north. The model has very little skill in reproducing summer precipitation variations in this region and what skill there is seems to come from the combined influence of Pacific and Atlantic SST.

It should be recognized that a climate model with this resolution (triangular truncation at zonal wavenumber 42 which translates into a horizontal grid with just less than 3° latitude and longitude spacing) cannot realistically be expected to accurately simulate precipitation in regions as small as those used here, given the small spatial scales and sharp gradients of precipitation fields. Instead,

the maps of observed and modeled SST-precipitation relationships (Figs. 1 through 4) make clear that the model does simulate the large scale patterns of precipitation teleconnections to the tropical Pacific and tropical North Atlantic, but that the smaller scale features, including the exact locations of the boundaries between positive and negative anomalies, are not as well represented. It is possible that methods of statistical or dynamical downscaling could be used to transfer the large scale simulations of precipitation anomalies produced by global climate models such as used here into more accurate regional simulations.

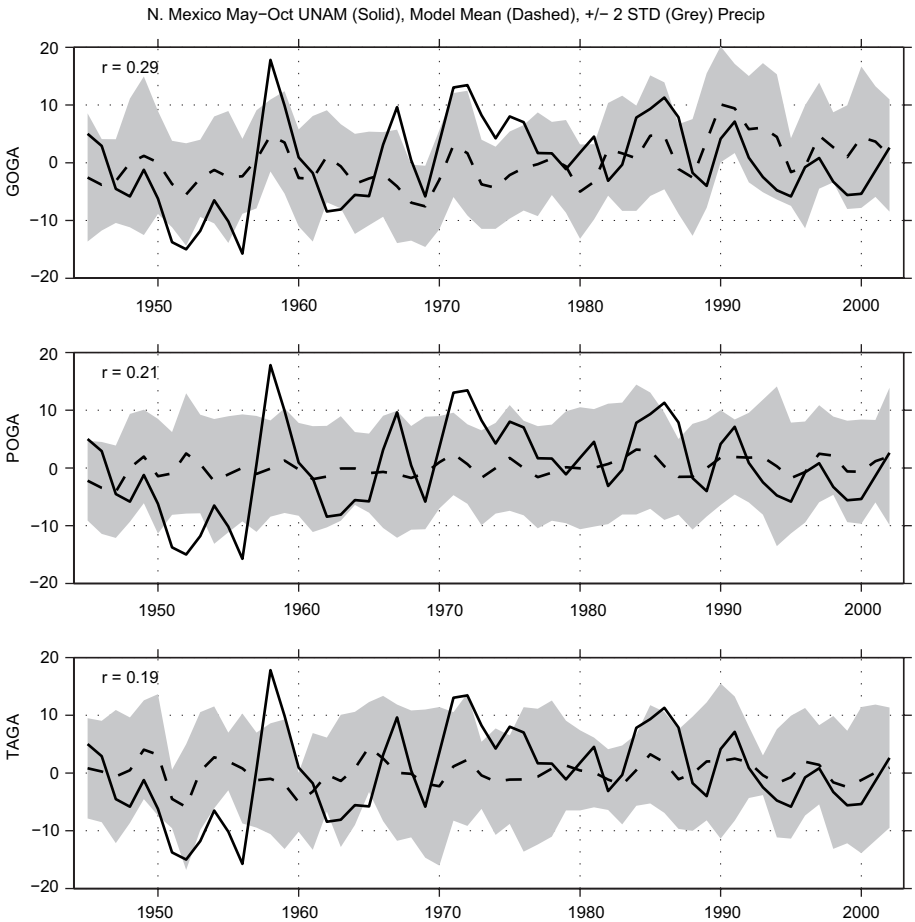

Fig. 7. Same as Fig. 5 but for the summer half year of the northern México region (all land areas in between 20° N and 30° N and 125° W and 95° W) and for the May through October half year.

6. Mechanisms for a summer half year ENSO impact on precipitation over the tropical Americas, Caribbean Sea and Gulf of México

The ability of the model to reproduce typical seasonal mean precipitation anomalies over the tropical Americas region associated with ENSO cannot easily be used to explain the mechanism by which this teleconnection occurs. The winter half year wetting of México and the Gulf of México during El Niño winters has been extensively studied using models and observations and is related to both the Pacific-North America Rossby wave teleconnection pattern (Trenberth *et al.*,1998) and

a more zonally-symmetric adjustment of the subtropical jet stream, eddy momentum fluxes and the eddy-driven mean meridional circulation (Seager *et al.*, 2003b, 2005a). Transient eddies are significantly involved in both processes. In contrast, summer half year links between the tropical Pacific and elsewhere are less well understood and, consequently, we will focus on that season here. Of particular interest is why the winter half year precipitation response to El Niño is very zonally symmetric but in summer the wet conditions are limited to the central and western United States and northern México and there is a wedge of dry conditions southeast of there that impacts southern México and Central America. Because of the northward migration and weakening of the storm track in summer relative to winter, transient eddy dynamics are expected to be less important, and tropical-subtropical teleconnections more important in the summer half year. Next we examine the summer teleconnections that influence hydroclimate anomalies over México and surrounding regions with a focus on the large scale dynamics rather than on the regional scale features of more direct relevance to México which the global model cannot be expected to capture.

6.1 The super-ensemble method for examining ENSO-forced tropical-subtropical teleconnections

The time scale for the atmosphere to adjust via wave propagation is on the order of days to less than a month. Hence to examine how a tropical SST anomaly impacts global climate we ideally need to examine the day by day response. This is not really possible using observational data because 1) the SST anomalies evolve on a timescale slower than the atmospheric adjustment timescale and therefore the SST-forced component of the atmospheric circulation is always in a quasi-equilibrium state and 2) the internal variability in the atmosphere on synoptic timescales can easily hide the SST-forced signal. Hence we turn to idealized experiments with the same climate model used above.

The approach we use will be termed a 'super-ensemble' and involves the following:

1. A 100 member ensemble of 100 day integrations beginning with different atmospheric and land surface initial conditions typical of June 1 and with climatological, time-varying, SST imposed thereafter. This is the 'climatology' ensemble.
2. A 100 member ensemble of 100 day integrations that begin from the same June 1 atmospheric and land surface initial conditions, but to which a typical El Niño SST anomaly for the June, July, August season is added to the SST boundary condition. This is the 'El Niño' ensemble.

Daily data is saved from all these ensembles. The 100 different initial conditions are chosen from long simulations with climatological SST. Since the same set of 100 different initial conditions is used to begin each 100 member ensemble, the time evolution of the corresponding ensemble members will be the same on the timescale of atmospheric weather predictability except for the influence of the different underlying SST boundary conditions. This is about 10 to 15 days. Averaging over the 100 ensemble members and then looking at the difference between the El Niño ensemble mean and the climatology ensemble mean clearly reveals the day by day evolution of the atmospheric circulation and precipitation patterns in response to the imposed SST anomaly (Lintner and Chiang, 2007), use a similiar methodology to examine the problem of tropical climate adjustment to El Niño). After the loss of atmospheric predictability averaging over the 100 ensemble members for a single day is not sufficient to clearly isolate the influence of the boundary forcing from the internal atmospheric variability. However, the SST boundary-forced signal becomes clear again when the difference between ensemble means is averaged over the entire

length of the simulations because this further suppresses the atmospheric internal variability that is uncorrelated between the ensemble members.

To understand the cause of the precipitation anomalies that develop within the super-ensemble we also compute the terms in the vertically integrated model moisture budget separately for each ensemble member using data on the model's hybrid-sigma vertical grid. The moisture budget terms were separated into a contribution from the change in circulation operating on the climatological humidity and a contribution from the climatological circulation operating on the change in humidity as well as the nonlinear cross term. It was found that the circulation change term was overwhelmingly dominant over the term involving the humidity change.

Figure 8 shows the precipitation and circulation contribution to the vertically integrated moisture divergence for the difference between the El Niño case and the climatological case, averaged over the 100 ensemble members for days 1, 3, 5, 7, 9, 11 and 13 and for the 100 day average. The increase in precipitation along the Equator in the Pacific, responding to warm SST anomalies, is clearly seen and develops throughout the 13 day period. As early as day 3 there is a decrease of precipitation in the region of northern South America and the Caribbean. As time develops the Atlantic sector drying expands northward so that in the 100 day average there is drying from northern South America to the Gulf coast of the United States and including southern México and all of Central America. A region of increased precipitation develops in the southern plains of the US reaching down into northern México at day 9 and is reasonably well established in the 100 day average. These patterns of modeled precipitation are quite realistic as compared to the observed patterns shown in Figure 2. It is important to note that these precipitation anomalies over the Atlantic sector arise in the absence of any underlying SST anomalies there.

The changes in precipitation are almost entirely accounted for by the change in moisture convergence or divergence forced by the change in circulation. In the region of precipitation reduction over the Caribbean Sea, Gulf of México and México and Central America subsidence forced from the Pacific creates a low level moisture divergence anomaly.

Figure 9 shows the time evolution of the 850 mb geopotential height anomaly. Low heights develop over the warm equatorial Pacific SST anomalies and also propagate eastward in a pattern symmetric about the Equator, the classic sign of an equatorial Kelvin wave. The wave takes about seven days to propagate around the globe (not shown). The pattern and phase speed are consistent with the first internal baroclinic Kelvin wave as in Gill (1980). It is the subsidence within the Kelvin wave that both causes the troposphere to warm and creates a low level moisture divergence anomaly that leads to suppressed precipitation to the east of the Pacific with an increase in moist static stability as the intermediate step (not shown, see also Lintner and Chiang, 2007).

Beginning around day 5, and well established in the 100 day mean, a low level high develops over the Gulf of México. Circulation around this high brings descent and dry conditions to its eastern flank over the Atlantic Ocean and ascent and wetter conditions to its western flank over northern México and the Plains, according to the Sverdup dynamics in Rodwell and Hoskins (2001) and Seager *et al.* (2003a). Relative high pressure in this region can arise as a combination of the Kelvin wave and Rossby wave response to the Pacific heating. The equilibrated response places low pressure along the equator to the east of the heating and, off the equator, to the northwest, of the heating. This places geostrophic southeasterly flow to the northeast of the center of the heating anomaly. Since the Pacific heating anomaly extends all the way to the coast of the Americas the southeasterly flow is over North America.

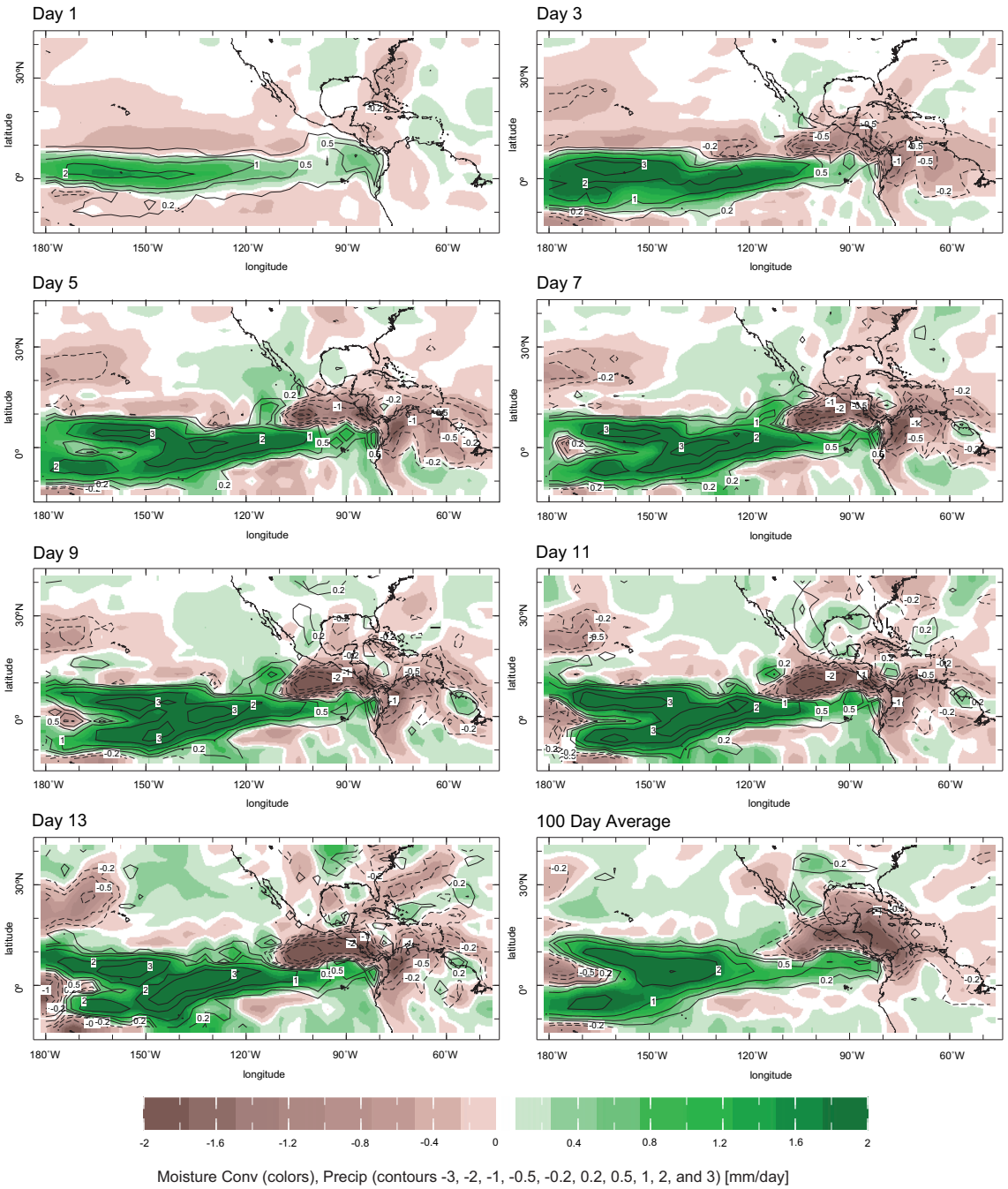

Fig. 8. The anomalies in precipitation (contours) and the contribution of anomalies in circulation to the anomalies of vertically integrated moisture convergence (colors) from the super-ensemble for the case of summer season El Niño minus climatological conditions. All results are averaged over 100 ensemble members for each of the two SST forcings with the 100 pairs of integrations beginning with the same 100 sets of atmospheric initial conditions. Results are shown at two day intervals from day 1 to day 13 as well as the 100 day average over the length of the integration. Units are mm per day.

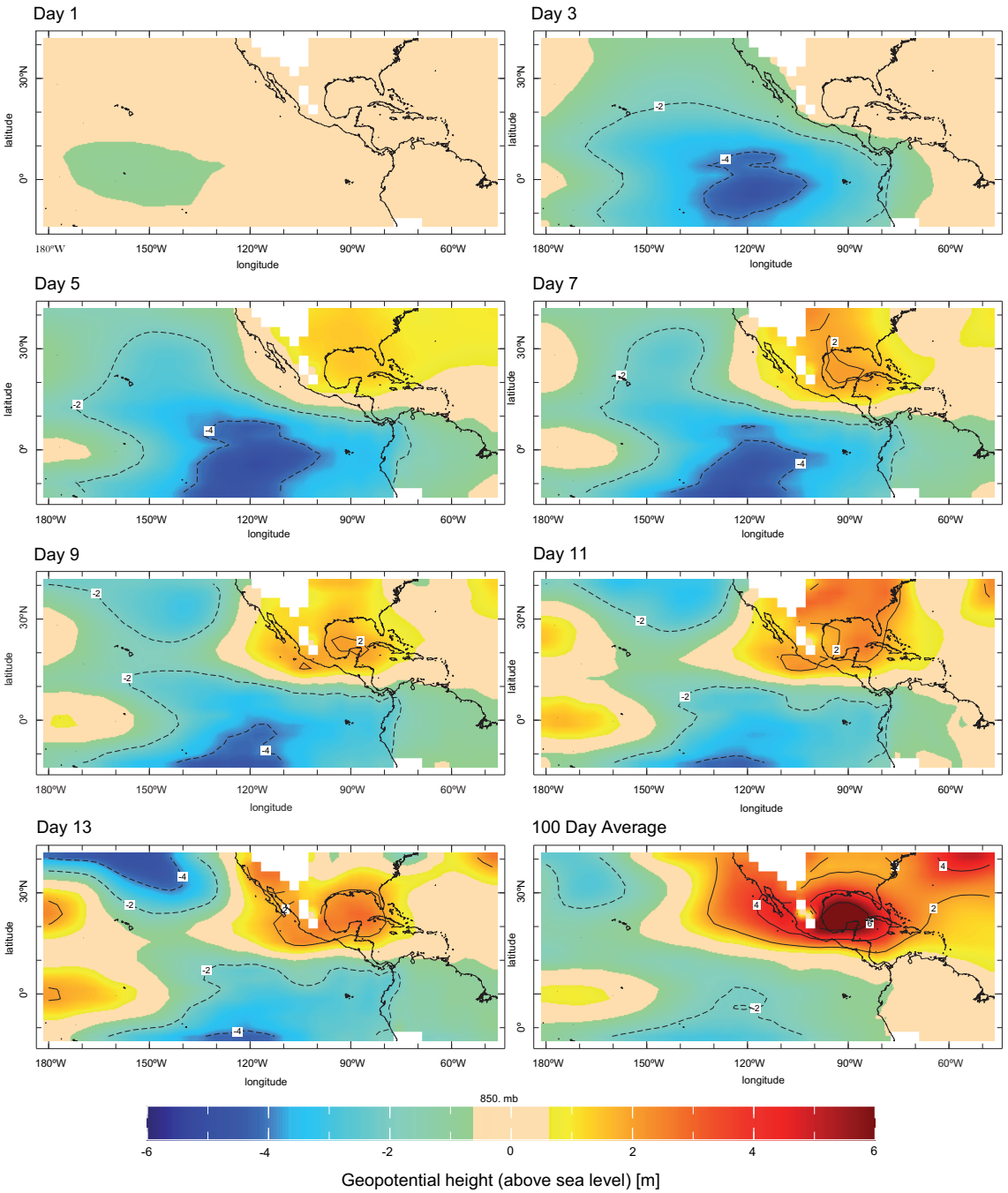

Fig. 9. The same as Fig. 7 but for the 850 mb height anomaly for summer between the El Niño run and the climatological run. Units are in meters.

6.2 ENSO forcing of circulation anomalies over the tropical and subtropical Americas: diagnosis with a forced linear model

The above argument explaining the precipitation anomalies over the subtropical Americas has so far invoked the response to the Pacific heating alone. However the suppressed precipitation and reduced heating over the tropical Atlantic could itself force a response that may contribute to the equilibrium circulation anomaly, in particular the Gulf of México low and the rising motion and wet conditions to its west. This cannot easily be determined by analyzing the day by day super-ensemble solution alone. It also cannot be analyzed with another SST-forced super-ensemble because the Atlantic heating anomalies arise independent of a change in underlying SST.

To examine this, we turn to experiments with a nonlinear dynamical model forced by imposed heating patterns that can separate out the responses to the Pacific and Atlantic heating anomalies. The model solves for perturbations relative to a specified June, July and August mean state accounting for interactions between the nonlinear terms. Application of Rayleigh friction, Newtonian damping and horizontal diffusion of vorticity, divergence and temperature prevents the solution from going baroclinically unstable before a nonlinear steady solution is arrived at. Details can be found in Ting and Yu (1998). The model is forced with the 100 day mean three dimensional total diabatic heating anomaly, El Niño case minus climatology, computed from the 100 day mean of the super-ensembles. The heating fields are regridded to the nonlinear stationary wave model grid (rhomboidal truncation at zonal wavenumber 15 and 12 vertical levels on a sigma coordinate).

Figure 10 shows the 850 mb geopotential height anomaly from the nonlinear model forced by the diabatic heating anomaly of the entire tropics (20° S-20° N). Unlike earlier plots here we show the results in the global domain to emphasize the difference between the solution in the northern and southern hemispheres. In the region of the tropical Americas and North America the model forced with all-tropics heating anomalies reproduces the low pressure at the equator and high pressure centered over the Intra-America Seas area and extending over to the Pacific Ocean that is seen in the mean of the 100 day integrations (Fig. 10). The strong signal of Rossby wave propagation from the tropics into the extratropics that is clear in the southern hemisphere is not seen in the northern hemisphere, suggesting that the circulation anomalies over the tropical-subtropical Americas arise from more tropical-subtropical processes.

The all-tropics heating anomaly includes positive heating over the Pacific Ocean and cooling over the equatorial Americas and Intra-America Seas region (Fig. 8). When the nonlinear model is forced by just the positive heating anomaly the Gulf of México high disappears (Fig. 10, middle panel). When the model is forced with the cooling in the tropical Americas-tropical Atlantic region the Gulf of México high reappears (Fig. 10, bottom panel). This is consistent with the Gill model response to an off-equatorial heating anomaly. In the region of cooling there is downward and equatorward motion (again by Sverdrup balance) and this leads to high pressure to the west and, on the other side of the forced anticyclone, poleward and rising motion that causes increased precipitation.

In combination with the results from the 100 day integrations these results make clear that a two step process is required to explain the summer circulation and precipitation anomalies over the Americas. First the Kelvin wave response to Pacific heating reduces precipitation in a broad region to the east. The precipitation and heating reduction is a maximum north of the equator because the climatological mean precipitation is there in this season. The forced negative heating anomaly in the tropical America sector itself forces a low level high to the northwest according to

a simple Gill model response. Circulation around the low level high creates increased precipitation to the west and sets up the wedge-shaped precipitation anomaly seen in the observations and GCM simulations forced by historical SST (Figs. 2 and 4).

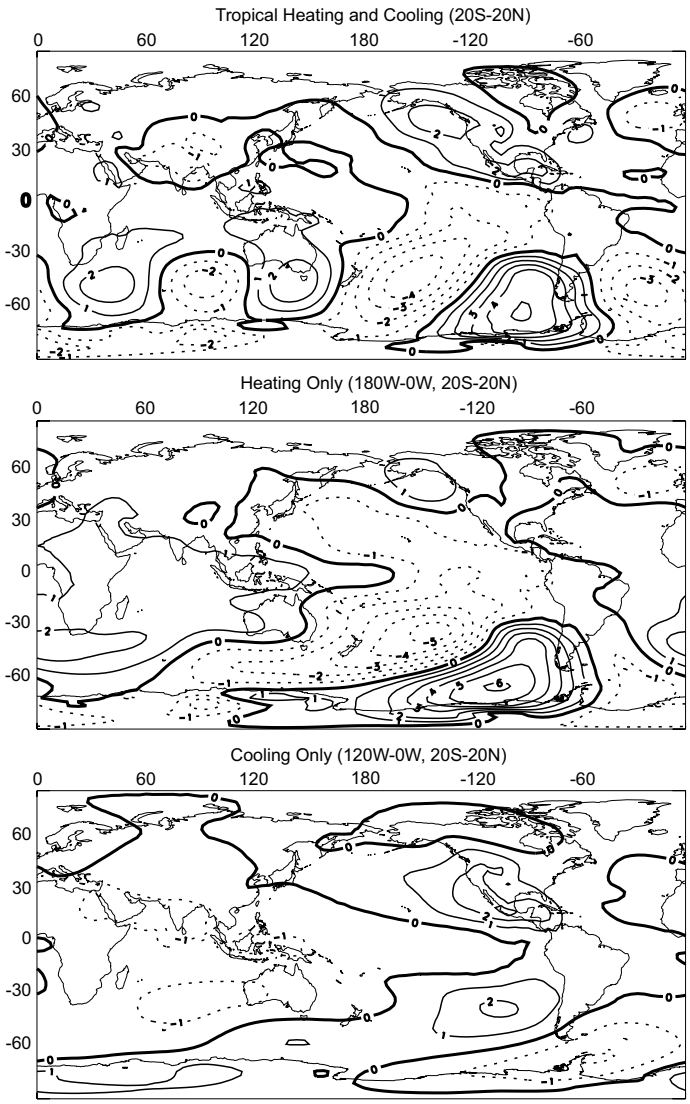

Fig. 10. The 850 mb geopotential height anomaly as simulated by a nonlinear primitive equation model forced by the three dimensional heating fields from the 100 day mean of the super-ensemble integrations. All results are for the summer season and for the El Niño heating minus the climatological heating. The top panel shows the response to heating anomaly throughout the tropics (20° S- 20° N), the middle panel shows the response to positive heating anomalies in the western hemisphere (eastward from 180° W to 0° W) and the bottom panel shows the response to negative heating (cooling) anomalies in the western hemisphere. See text for more details. Units are in meters.

7. Modeled and tree ring-reconstructed Mexican drought during the period of instrumental SST observations

Instrumental, ship-based, observations of SST with near global, but spatially sparse, coverage begin in 1856. The model simulations used here begin in January 1856 and allow an assessment of the extent to which SST forcing explains Mexican hydroclimate in the ensuing 150 years. Instrumental precipitation and temperature data, however, are very sparse before the middle of the last century. Hence we turn to tree ring records of hydroclimate as contained within the North American Drought Atlas (NADA). The NADA presents a gridded record of summer Palmer Drought Severity Index (PDSI) reconstructed from tree ring records from México, the United States and Canada (Cook *et al.*, 2004, 2007) and extended to 2005 with instrumental PDSI from Dai *et al*. (2004). Over México the records go back into the fourteenth century but at no time cover that part of México east of 95° W which includes the Yucatán peninsula.

The tree ring widths depend in large part on the moisture conditions during the spring and summer growing season but this in turn depends on precipitation and evaporation during preceding seasons. To simplify matters we will compare the tree ring records to annual mean modeled moisture conditions restricting our attention to northern México (as defined above) because of the better tree ring data coverage there and because the SST-forced signal there has the same sign year round. Since PDSI is a proxy for soil moisture conditions, we compare it to the modeled soil moisture anomaly in the upper 0.7 m of the soil. (The conclusions are not appreciably changed when comparing the tree ring reconstructions to spring to summer modeled soil moisture.)

Figure 11 shows time series of the tree ring-reconstructed PDSI and the annual mean modeled soil moisture for the GOGA model after 3 year low pass filtering. There is modest agreement between modeled soil moisture and tree ring-reconstructed PDSI during the entire period. In particular there were two large amplitude, multiyear dry periods around 1910 (during the Mexican revolution) and 1917 that were separated and flanked by multiyear wet periods that are well captured by the model. The tree ring records show a strong multiyear drought during the early to mid 1890s, which is not simulated well by the model with global SST forcing, and a weaker drought in the early to mid 1860s which is simulated but underestimated by the model. Both of these droughts also had serious impacts in the United States (Stahle and Cleaveland, 1988; Herweijer *et al.*, 2006).

In the earlier modeling work of Herweijer *et al.* (2006) and Cook *et al.* (2007) the 1850s-1860s and the 1890s drought were attributed to multiyear La Niña events. The GOGA model, which also includes Atlantic SST-forcing, fails to produce the 1890s drought because the observed Atlantic SST were cold at this time and, hence, in the model, this forced wet conditions in southwestern North America. This is clearly shown by the other time series in Figure 10 which shows results from the model with tropical Pacific SST forcing alone and coupled to a mixed layer ocean model elsewhere (POGA-ML). This model does produce a multiyear drought in the 1890s. Apparently both the 1890s and 1850s-1860s drought were year round droughts since they also appear in reconstruction of winter precipitation for the Durango region of northern México by Cleaveland *et al*. (2003) and for northeastern México by Villanueva-Díaz *et al*. (2007) (as does the 1950s drought).

Despite the absence of instrumental precipitation records, abundant documentation and tree ring records leave no doubt that there was a serious drought in northern México in the 1890s. For example under the heading of 'Starvation in Durango. Distress Caused by the Long Continued Drought in Mexico' The New York Times wrote on December 17, 1891: "The distress among the people of this city and throughout the State of Durango, on account of the drought, is on the

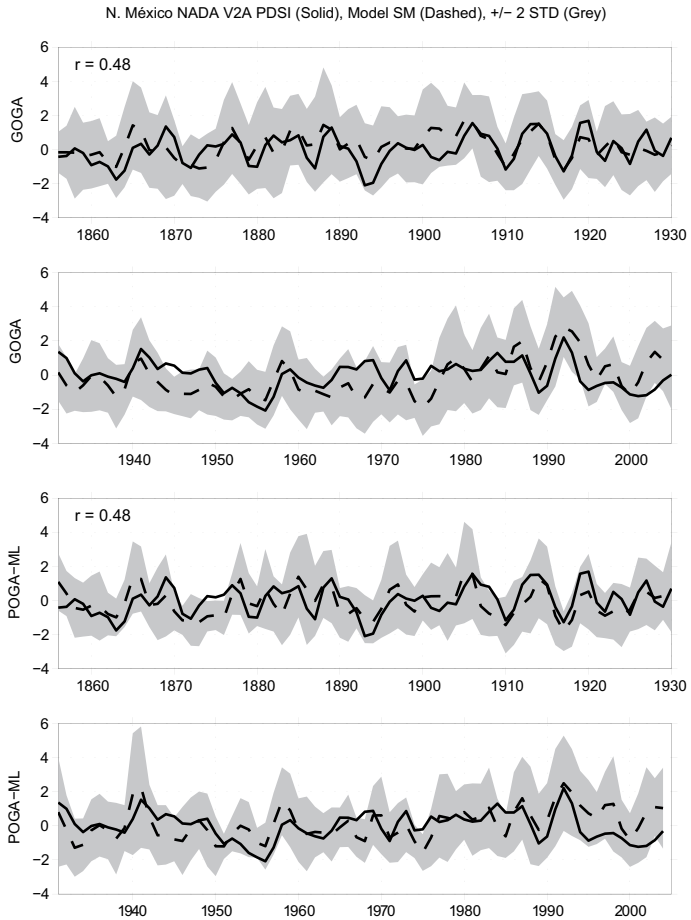

Fig. 11. The tree ring-reconstructed PDSI and the modeled soil moisture with (top) global SST forcing and (bottom) tropical Pacific SST forcing alone and a mixed layer ocean elsewhere, average over northern México, for the 1856 to 2004 period. The time series are standardized and have been smoothed with a 3 year low pass filter. The shading is the two standard deviation spread of the model ensemble.

increase. The suffering among the lower classes cannot be described. It is a famine of the worst kind, and the pleadings and cries of the hungry horde for food is becoming louder with each succeeding day."

And then, two years later, under the heading 'Suffering from drought in México' the New York Times published on May 15, 1893 the following reporting on conditions in the northern Mexican state of Sonora: "There is great suffering and destitution among the lower classes in the Altar mining district, this state, owing to the severe drought that has prevailed there almost four years. All of the mountain streams, springs, and wells are dry, and the water must be hauled from the village of San Antonio, a distance of twenty-five miles. The precious fluid retails at 8 per barrel. The poor people cannot afford to pay that price, and many of them have been living for several weeks on the nourishment obtained from the maguey plant, which grows in abundance in that section, and flourishes best in time of drought."

Figure 12 shows maps of the tree-ring reconstructed PDSI and POGA-ML modeled soil moisture anomaly during the 1890s drought for all of North America. Dry conditions stretched from southern México to Canada and from the western slope of the Rockies to the Atlantic with just the Pacific coast of the United States and the northeast wet, a pattern that is reasonably well represented by the model. It must be noted that PDSI is constructed to be a measure of soil moisture variations that attempts to normalize using climatological values. Consequently we do not expect PDSI and modeled soil moisture amplitudes to have the same regional variations. Figure 12 also shows maps of the other severe drought in the post 1856 period that impacted Mexico during the early to mid 1950s. Once again the drought impacted most of México and extended over a large area of North America, but there were wet conditions across parts of the northern United States and southern Canada. The GOGA modeled 1950s drought also impacted almost all of Mexico but the wet conditions in the northern United States and Canada were not simulated. Unlike the 1890s drought, the 1950s drought in the model was created by both a La Niña and a warm subtropical North Atlantic Ocean (not shown but see Seager *et al.,* 2008a).

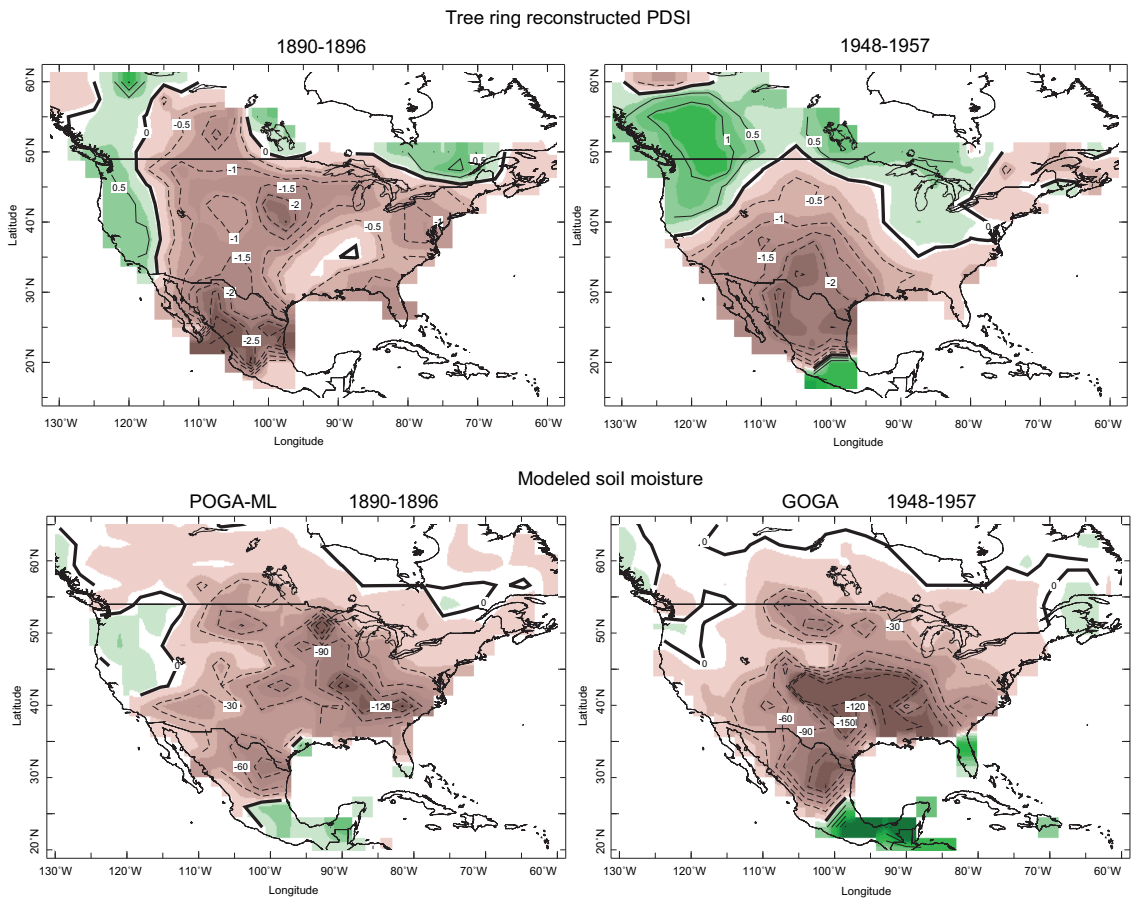

Fig. 12. The tree ring-reconstructed PDSI and the modeled soil moisture anomaly for the 1890 drought (left) and the 1950 drought (right). The modeled 1890 drought is for the case with tropical Pacific SST forcing and a mixed layer ocean elsewhere and the modeled 1950 drought is for the case with global SST forcing. The modeled soil moisture is in mm.

Given that the 1890s drought occurred and it was during a concurrent La Niña, and given that the model with global SST forcing did not simulate it, either the model's response to the tropical Atlantic SST anomalies is too strong relative to its response to tropical Pacific SST, or the SST data erroneously indicates a cold Atlantic in the 1890s. We cannot resolve that issue here but simulations conducted with different models, that may have different sensitivities to SST in the tropical oceans, would be of help.

8. Modern Mexican droughts in the context of tree ring-reconstructed drought since 1380 A.D.

The tree ring records provide the opportunity to examine the droughts that occurred within the period of instrumental observations in the context of much longer periods of hydroclimate variations. Figure 13 shows the tree ring reconstructed PDSI averaged over northern México (as defined above) from 1380 A.D. to 2006. Although there are records before 1380 A.D. this start date is chosen to ensure reasonable data coverage. The data have been smoothed with a six year low pass filter. The 1950s drought stands out as the drought with the largest amplitude within these centuries. However, the worst overall drought appears to be the late sixteenth century 'megadrought' that also impacted the area of the modern United States and parts of modern day Canada (Stahle *et al*., 2000; Cleaveland *et al.*, 2003; Stahle *et al.*, 2007) and which is remarkable not for its amplitude but for its duration. It has been argued that this drought aggravated the hemorrhagic fevers that caused the native population collapse in the 16th Century México (Acuña-Soto *et al.*, 2002). The causes of the sixteenth century drought are, however, entirely unknown.

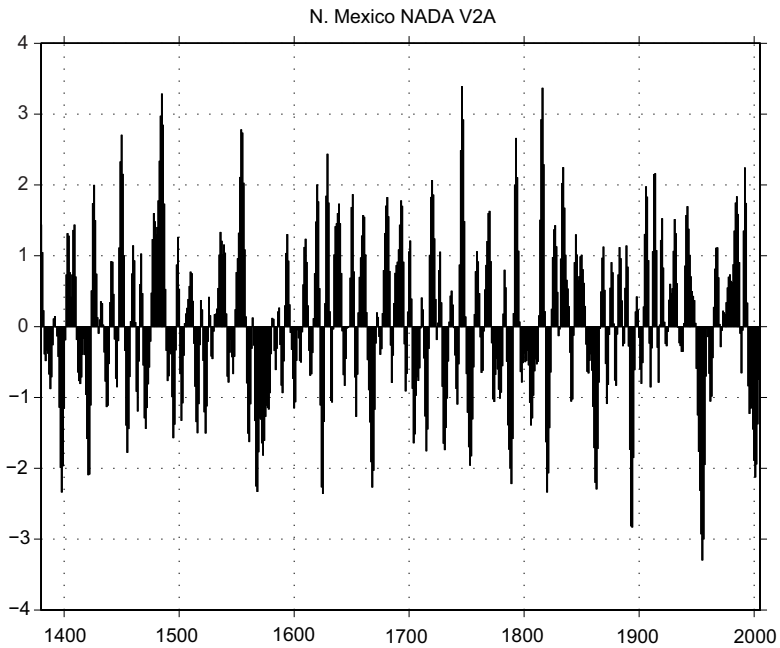

Fig. 13. The tree ring-reconstructed PDSI over northern México for 1380 to 2005 after smoothing with a six year low pass filter. Negative values stand for dry conditions and positive for wet conditions.

As seen in Figure 14 this drought was extraordinarily widespread, extending from central México to Canada and from the Pacific to the Atlantic but with maximum severity in northern and central México. According to this multi-centennial record for northern México, even though the drying trend over the last two decades is clear, the late twentieth to early twenty-first century drought looks much like droughts that have occurred before. There is no sign of a long multidecadal or multicentennial trend in the drought index although one needs to be cautious since the statistical methods used to convert the tree ring chronologies into climate records can attenuate such long term variations.

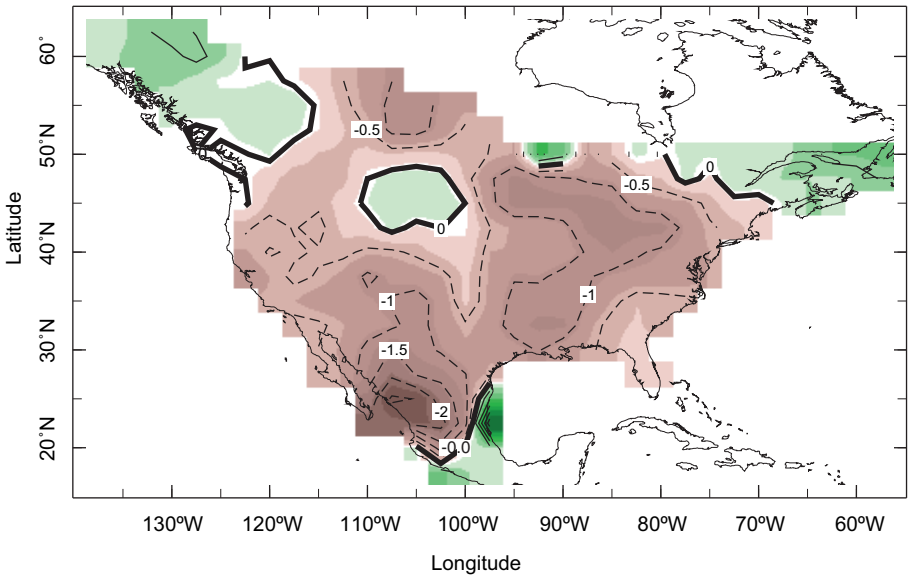

Fig. 14. The tree ring-reconstructed PDSI average over 1559 to 1582 A. D., the 16th Century megadrought.

9. Is Mexican hydroclimate changing?

Simulations of changes in climate forced by changes in radiative forcing from both natural and human causes indicate that global warming induces a drying of México and the southwestern United States that begins in the late 20th Century and continues through the current century (Seager *et al*., 2007a). The projections of increased aridity are quite robust in that almost all models project a drying in the region, as part of a general drying of the subtropics (Held and Soden, 2006; Seager *et al.*, 2007a). It is important to determine if there is evidence that this projected drying is already occurring.

To do this we build on the previous identification of a drought over northern México that has stretched from the early to mid 1990s at least through the early part of the current decade (Hallack- Alegría and Watkins, 2007). This drought is evident in Figure 7 (top panel) for the summer season precipitation over northern México and in Figure 5 for the winter season precipitation for all of México. Southern México during the summer season has not seen a recent drying according to the UNAM data. Winter drying is reproduced by the climate model with tropical Pacific SST forcing alone indicating that this is in part related to a transition during the last decade and a half to a more La Niña-like tropical Pacific (Seager, 2007). Despite this identification of a post early 1990s drought it is not obvious from the figures already presented that there is a long term drying trend.

However to look more closely we compute differences in precipitation for the period extending from 1993 until the end of the data sets relative to the period up through 1992. In addition to the data sets and model simulations already used we analyze the average across a 24 member ensemble of simulations of twentieth century and projections of twenty-first century climate forced by known or estimated and projected changes in radiative forcing. These simulations were done as part of the Intergovernmental Panel on Climate Change Assessment Report Four (IPCC AR4).

The observed difference between the post 1993 period and the earlier period according to the UNAM data set (Fig. 15, using a base period from 1945 to 1992) shows a drying of northern México but not of southern México. Over the United States there is some evidence of drying in the Rocky Mountain States and a shift to wetter conditions on the Pacific coast and in the Mississippi valley and to drier conditions in the southeast. These patterns are reasonably well reproduced by the change in PDSI from the NADA data (Fig. 15). However it should be noted that for recent decades the NADA data set is heavily influenced by the Dai *et al*. (2004) instrumental PDSI because so many tree records do not extend this late. The Dai's data suffers from the drop off of Mexican station data but nonetheless agrees with the more complete UNAM data on drying in the last decade. The UNAM temperature data shows no warming trend over this period (not shown) indicating that the recent drought was driven by a precipitation reduction. Consistently, Englehart and Douglas (2005) show that daily maximum temperatures increased over the post 1970 period but decreased in prior decades leading to essentially no trend over the post 1945 period analyzed here. Over the same time period the AR4 models simulated a radiatively-forced climate change that had weak drying across most of México and the southwestern United States, but within a spatial pattern that is distinct from the observed change.

The availability of satellite-derived precipitation data sets begin in the late 1970s. These have the advantage of continuous global coverage and could potentially be useful where weather station records are limited. Also shown in Figure 15 is the difference in satellite-derived precipitation, from the CAMS Outgoing Longwave Radiation Precipitation Index (OPI), a purely satellite data set, for 1993-2006 relative to 1979 to 1992. This data, independent of the UNAM station data and the NADA PDSI, also shows a drying of México apart from its southern regions. But once again the AR4 simulation of radiative-forced change over this shorter period (also shown in Fig. 15) has a pattern dissimilar from that observed.

Finally, the IPCC AR4 multimodel ensemble mean precipitation change across a longer period, between 2021-2040 relative to 1945-2000 is also shown in Figure 15. This shows a very clear drying of all of México, Central America and the southwestern United States (as discussed in Seager *et al*., 2007a). This pattern is very similar to the IPCC AR4 model simulation change for the earlier period shown in Figure 15 but the magnitude is much greater. By drying all of México the pattern of anthropogenic drying is distinct from the patterns of natural variability which, with the exception of the Pacific influence during the winter half year, tends to affect northern and southern México in contrasting ways. Consequently anthropogenic climate change will lead to increased likelihood of 'all México droughts'. During the winter half year this will be caused by a less southward placement of the winter storm track and jet stream, and in the summer half year by a weakening and less northward movement of the Central America-southern México tropical convection zone.

The pattern of observed hydroclimate change across North America does not clearly match the pattern simulated by the IPCC models as a response to changes in radiative forcing. This is prob-

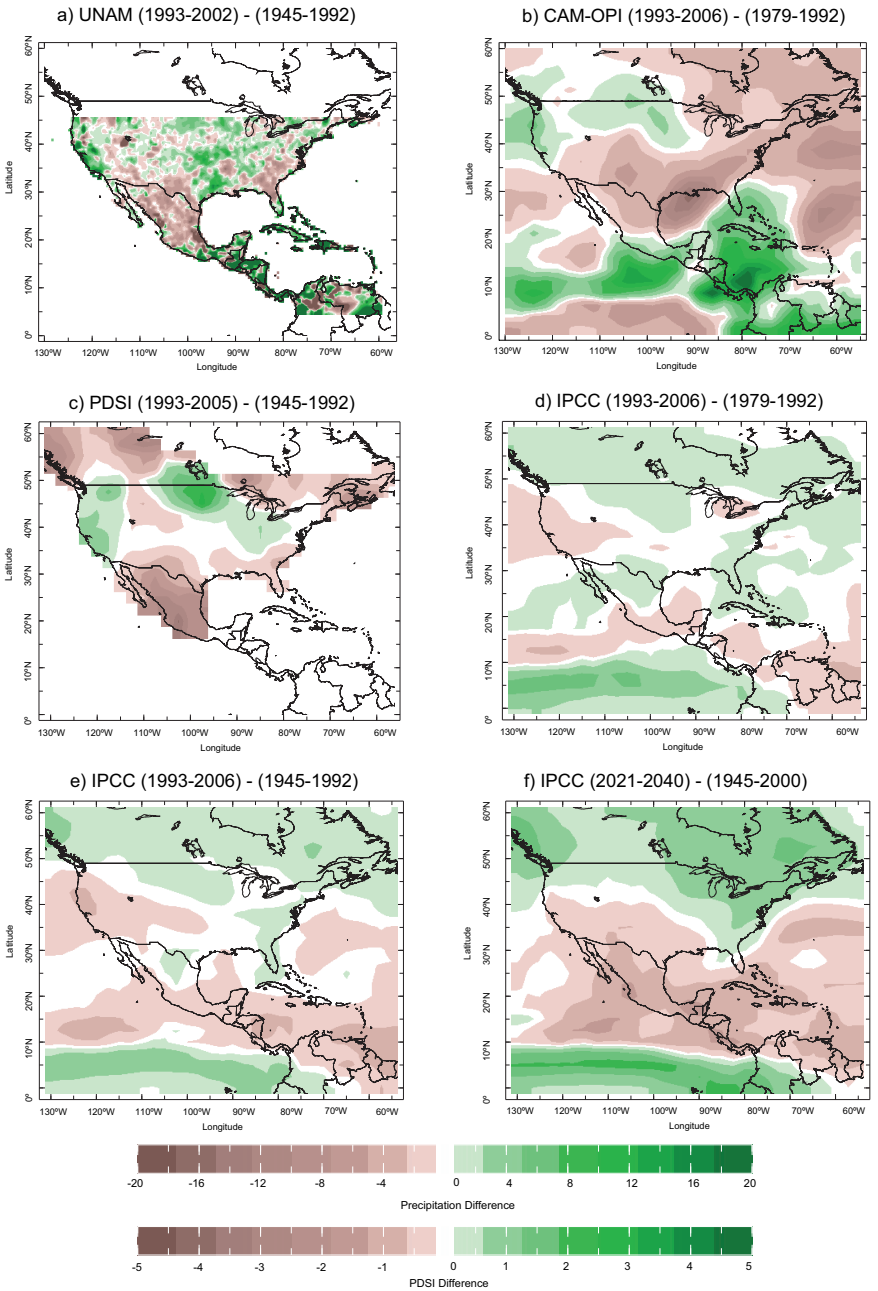

Fig. 15. Various time differences in annual mean hydroclimate fields. The difference between the post 1993 period and the 1945 to 1992 period for UNAM precipitation observations (top left) and in the multimodel ensemble mean of IPCC AR4 model precipitation simulations (bottom left) and PDSI from tree ring records extended with instrumental data (middle left). The difference between the post 1993 period and the 1979 to 2002 period for satellite derived precipitation from CAMS (top right) and the multimodel ensemble mean of IPCC AR4 precipitation simulations (middle right). The IPCC AR4 multimodel ensemble mean precipitation difference between the 2021 to 2040 period and the 1945 to 2000 period (bottom right).

ably because the observations contain significant natural variability in addition to any externally forced climate change.

For example, when computing trends or differences over the second half of the twentieth century the results are inevitably influenced by the 1976/77 climate shift in the Pacific Ocean (Graham, 1994; Trenberth and Hurrell, 1994). As shown by Huang *et al.* (2005), this shift to a more El Niño-like tropical Pacific caused the mid-latitude and subtropical Americas to become wetter. This tropical SST-induced change could mask or overwhelm any subtropical anthropogenic drying during the same time interval. However, computing differences across 1993, as done here, should reduce the impact of the Pacific shift and, indeed, the differences in Figure 14 do not look like the differences across 1977 in Huang *et al.* (2005) that show a shift to a wetter subtropics and mid-latitudes.

For the shorter time period of the satellite era differences or trends can also be influenced by the difference between the pre-1998 and post-1998 period which may be a shift to a more La Niña like state of the tropical Pacific –i.e. opposite to the 1976/77 shift– although it is too early to tell. It is plausible that such shifts between states that last for decades are of natural origin (Karspeck *et al.*, 2004; Seager *et al.*, 2004). The post-1998 drying of northern Mexico and the southwestern United States, while broadly consistent with the general IPCC AR4 simulations, is also consistent with a more La Niña-like state post 1998. However the attempt to distinguish between La Niña- and anthropogenic-induced drying is confounded if positive radiative forcing causes a shift to a more La Niña-like state of the tropical Pacific (Clement *et al.*, 1996; Cane *et al.,* 1997; Cane, 2005; Mann *et al.*, 2005; Cook *et al.*, 2007; Emile-Geay *et al.,* 2007).

10. Social impacts of recent and projected Mexican drought

Although the most recent drought may not have been worse than the 1950s drought it has happened in a quite different social and economic environment. The most recent drought came on the heels of far-reaching structural changes in the Mexican economy and agriculture arising from the North American Free Trade Agreement (NAFTA) and amidst ongoing privatization of formerly communal land and water rights (Wilder and Lankao, 2006). NAFTA stimulated industrial growth in the semi-arid north and encouraged commercial farmers to move toward alfalfa and export crops, especially fruits and vegetables, that are all water intensive (Liverman, 1999) while the 1992 reform of Mexico's basic hydraulic law opened the door to market-based water pricing (Wilder and Lankao, 2006). In the face of protracted drought and rising water demand by export-oriented fanners, border industrial plants ('maquiladoras') and growing cities in northern Mexico, numerous 'water wars' were initiated between different communities and user groups, including an international conflict over Chihuahua's inability to supply downstream Texan farmers with treaty-allocated Rio Bravo/ Grande water (Pearce, 2006).

Although initial impacts were felt by small cattle ranchers, traditional corn growers, and indigenous communities in the Sierra Madre Occidental, the entire northern Mexico economy soon felt the repercussions of drought. By mid-summer 1996, most major reservoirs were below 20 percent of capacity, nearly two million acres of farmland went uncultivated for lack of water and Mexican grain inputs jumped sharply (Liverman, 1999). Since NAFTA was implemented and the drought began there has been a decline in both the numbers of farmers in Mexico and in agricultural employment and continued out-migration from rural areas (USDA, 2006). While it is difficult to disentangle the impacts of NAFTA, water law reform and climate, newspapers reported that the

drought led to migration of rural inhabitants to border cities and into the United States (see articles in La Jornada, a leading daily newspaper in México City, on 22 May and 13 August 2000). The impacts of the drought on small and traditional, communal landholders were exacerbated by the 1992 reform of the water law which caused an increase in water prices (Wilder and Lankao, 2006). The major social and economic changes in Mexican agriculture over the last decade and a half are the combined result of severe climate-induced stress occurring in combination with the increased exposure of Mexican agriculture to the United States economy by the economic changes brought about by NAFTA and market-based reform of Mexican water law.

The recent drought has primarily affected northern México but global warming-associated climate change is projected to cause drying of the whole of México. If the base climatology of México is changing, the most vulnerable region may actually be the 13 states of Central México that sit between the semi-arid region to the north and the wetter climate to the south. This region has the highest population density in México and includes México City with a vast water use that is already depleting regional aquifers and watersheds (CNA, 2006). Even as warming here may lengthen the growing season (Conde *et al.*, 2006) the projected drying of this region both in winter, by an intensified atmospheric moisture divergence and a poleward expanded subtropical dry zone, and in summer, by a weaker Mexican monsoon, will add further stress to water resources and could lead to ecological change and negative impacts on agriculture and to economic instability (Martínez and Fernández, 2004).

11. Conclusions

We have examined instrumental records, model simulations forced by historical and idealized SSTs, proxy tree ring records and model simulations and projections ofradiatively-driven climate change to better understand the causes of Mexican hydroclimate variability and change. The study leads to the following conclusions:

1. Analysis of observations and models show that an important component of variations in Mexican hydroclimate is controlled by variations in tropical Pacific and tropical Atlantic SSTs. During the winter half year the whole of México is wet during El Niño, while the influence of the Atlantic Ocean is negligible. In the summer half year. El Niño conditions make northern México wet but southern México dry. For southern México the summer teleconnection is stronger than in winter. Consequently, in northern México ideal conditions for drought are a La Niña and a warm subtropical North Atlantic and vice versa for southern México.
2. Tree ring reconstructed summer PDSI in northern México since the mid nineteenth century is quite well tracked by soil moisture in an atmosphere model forced by the entire history of observed SSTs with a clear indication of the influence of tropical Pacific SSTs. The severe 1950s drought is well captured by the model with both tropical Pacific and Atlantic forcing, while the devastating 1890s drought is only captured in the model with tropical Pacific SST forcing alone, the implications of which need to be resolved.
3. Super-ensembles of short integrations forced by a sudden imposition of an El Niño SST anomaly are used to explain the wedge of reduced summer season precipitation over the heating over the tropical Pacific and propagating east as a Kelvin wave. Descent causes both atmospheric warming and low level moisture divergence stabilizing the column to convection and reducing the precipitation. The Pacific-induced negative heating anomaly over the northern tropical Atlantic

forces a low level high pressure anomaly to its northwest as in Gill (1980). Flow around this high places southerly flow over northeast México and the southern Plains forcing increased precipitation there.

4. Analysis of tree ring records for northern México going back to 1380 A. D. shows that droughts as severe as those of the 1890s, 1950s and in recent years have occurred throughout the last several centuries. The late sixteenth century megadrought (Stahle *et al.*, 2000) stands out but not so much for its severity as for its longevity.
5. Climate models project all of México to become drier early in the current century as a result of anthropogenic warming (Seager *et al.,* 2007a), but analyses of changes in precipitation over the late twentieth century and the current decade do not unequivocally demonstrate that this is already occurring, potentially because natural variations (caused by variations of tropical SSTs) are sufficiently large to mask a developing anthropogenic signal.

The inability to prove that Mexican hydroclimate is already changing as a consequence of global warming should not lead to any drop in concern about climate change. As shown in Seager *et al*. (2007a), the drying of southwestern North America is a very robust prediction of climate models. This is because it is caused by 1) an intensified atmospheric hydrological cycle caused by rising humidity and 2) a poleward expansion of the Hadley Cell and poleward movement of the mid-latitude jet stream and storm tracks. The robustness probably comes from these being large scale processes that follow from overall warming that are not dependent on particular patterns of SST change. However, as Seager *et al.* (2007a) show, the median projected drying turns the mean climate into a level of aridity akin to, say, the 1950s drought sometime between now and the middle of the century. An inability to unambiguously identify this trend as of now is not inconsistent with such a prediction.

Unfolding climate events need to be closely monitored for evidence that they are caused by either natural variability or anthropogenic climate change. The differences in the mechanisms and the associated patterns of SST change should provide the means to do this using dynamical models and analysis of observations. However, even as we wait for the irreversible aridification of México to become apparent, natural variability will continue to occur and it will be possible to use these modes of variability to predict aspects of summer and winter half year hydroclimate variations throughout México.

Acknowledgement

The work was supported by NOAA grants NA030AR4320179 PO7 and 20A and NSF grants ATM-0347009 and ATM-0501878. We thank Cyrus Veeser for translating the abstract, Claudia Giulvi for additional help with translation and the comments and suggestions of two anonymous reviewers. The model simulation data can be accessed online at: http://kage.ldeo.columbia.edu:81/ \newline SOURCES/.LDEO/.ClimateGroup/.PROJECTS/.CCM3, Lamont Doherty Earth Observatory Contribution Number 7201.

References

Acuña-Soto R., D. W. Stable, M. K. Cleveland and M. D. Therrell, 2002. Megadrought and megadeath in 16th Century México. *Emerg. Infect.* Dis. **8**, 60-362.

Cane M. A., 2005. The evolution of El Niño, past and future. *Earth Plan. Sci. Lett.* **230**, 227-240.

Cane M. A., A. C. Clement, A. Kaplan, Y. Kushnir, D. Pozdnyakov, R. Seager, S. E. Zebiak and R. Murtugudde, 1997. Twentieth Century sea surface temperature trends. *Science* **275**, 957-960.

Cleaveland M. K., D. W. Stahle, M. D. Therrel, J. Villanueva-Diaz and B. T. Bums, 2003. Tree-ring reconstructed winter precipitation and tropical teleconnections in Durango, México, *Clim. Change* **59**, 369-388.

Clement A. C., R. Seager, M. A. Cane and S. E. Zebiak, 1996. An ocean dynamical thermostat. *J. Climate* **9**, 2190-2196.

Conde C., R. Ferrer and S. Orozco, 2006. Climate change and climate variability impacts on rain-fed agricultural activities and possible adaptation measures. A Mexican case study. *Atmósfera* **19**, 181-194.

Cook E. R., C. Woodhouse, C. M. Eakin, D. M. Meko and D. W. Stable, 2004. Long term aridity changes in the western United States. *Science* **306**, 1015-1018.

Cook E. R., R. Seager, M. A. Cane and D. W. Stable, 2007. North American droughts: Reconstructions, causes and consequences. *Earth. Sci. Rev.* **81**, 93-134.

CNA, 2006. Estadísticas del agua en México. Sistema Nacional de Información sobre Cantidad, Calidad, Usos y Conservación del Agua, Comisión Nacional del Agua, México, D. F., 201 pp.

Dai A., K. E. Trenberth and T. Qian, 2004. A global dataset of Palmer drought severity index for 1870-2002: Relationship with soil moisture and effects of surface wanning. *J. Hydrometeorol.* **5**, 1117-1130.

Emile-Geay J., M. A. Cane, R. Seager, A. Kaplan and P. Almasi, 2007. ENSO as a mediator for the solar influence on climate. Paleoceanogr. 22, doi: 10.012972006PA001304.

Englehart P. J. and A. V. Douglas, 2002. México's summer rainfall patterns and analysis of regional modes and changes in their teleconnectivity. *Atmósfera* **15**, 147-164.

Englehart P. J. and A. V. Douglas, 2005. Changing behavior in the dirunal range of surface air temperatures over Mexico. Geophys. *Res. Lett.* **32**, doi: 10.102972004GL021139.

Gill A. E., 1980. Some simple solutions for heat induced tropical circulation. *Q. J. R. Meteorol. Soc.* **106**,447-462.

Graham N., 1994. Decadal-scale climate variability in the tropical and North Pacific during the 1970s and 1980s: observations and model results, *Clim. Dyn*. **10**, 135-162.

Graham N., M. K. Hughes, C. M. Ammann, K. M. Cobb, M. P. Hoerling, D. J. Kennett, J. P. Kennet, B. Rein, L. Stott, P. E. Wigand and T. Xu, 2007. Tropical Pacific-mid latitude teleconnections in medieval times, *Clim. Change* **83**, 241-285.

Hallack-Alegría M. and D. W. Watkins, 2007. Annual and warm season drought intensity-duration-frequency analysis for Sonora, México. *J. Climate* **20**, 1897-1909.

Held I. M. and B. J. Soden, 2006. Robust responses of the hydrological cycle to global warming. *J. Climate* **19**, 5686-5699.

Herweijer C., R. Seager and E. R. Cook, 2006. North American drought of the mid to late nineteenth Century: History, simulation and implications for medieval drought. *The Holocene* **16**, 159-171.

Herweijer C., R. Seager, E. R. Cook and J. Emile-Geay, 2007. North American droughts of the last millennium from a gridded network of tree ring data. *J. Climate* **20**, 1353-1376.

Huang J., R. Seager and Y. Kushnir, 2005. The 1976/77 transition in precipitation over the Americas and the influence of tropical SST. *Clim. Dyn. 24*, 721-740.

Janoviak J. E. and P. Xie, 1999. A global satellite-rain gauge merged product for realtime precipitation monitoring applications. *J. Climate* **12**, 3335-3342.

Kaplan A., M. A. Cane, Y. Kushnir, A. C. Clement, M. B. Blumenthal and B. Rejagopolan, 1998. Analysis of global sea surface temperature: 1856-1991. J. Geophys. Res. 103, 18567-18589.

Karspeck A., R. Seager and M. A. Cane, 2004. Predictability of tropical Pacific decadal variability in an intermediate model. *J. Climate* **17**, 2842-2850.

Kiehl J. T., J. J. Hack, G. B. Bonan, B. A. Bovile, D. L. Williamson and P. J. Rasch, 1998. The National Center for Atmospheric Research Community Climate Model: CCM3. *J. Climate* **11**, 1131-1149.

Lintner B. R. and J. C. H. Chiang, 2007. Adjustment of the remote tropical climate to El Niño Conditions. *J. Climate* **20**, 2544-2557.

Liverman D. M., 1999. Vulnerability and adaptation to drought in México. *Nat. Res. J.* **29**, 99-115.

Lu J., G. Vecchi and T. Reichler, 2007. Expansion of the Hadley Cell under global warming. *Geophys. Res. Lett.* **24**, doi:10.1029/2006GL028443.

Mann M., M. A. Cane, S. E. Zebiak and A. Clement, 2005. Volcanic and solar forcing of the tropical Pacific over the past 1000 years. *J. Climate* **18**, 447-456.

Martínez J. and A. Fernández (Compiladores), 2004. *Cambio climático: una visión desde México.* Instituto Nacional de Ecología, México, D. F., 525 pp.

Mitchell T. D. and P. D. Jones, 2005. An improved method of constructiong a database of monthly climate observations and associated high resolution grids. *Int. J. Climatol.* **25**, 693-712.

Pearce F., 2006. *When the rivers run dry: Water-the defining crisis of the twenty-first Century*. Beacon Press, Boston, 324 pp.

Rayner N., D. Parker, E. Horton, C. Folland, L. Alexander, D. Rowell, E. Kent and A. Kaplan, 2003. Global analyses of sea surface temperature, sea ice and night marine air temperature since the late nineteenth century. *J. Geophys. Res.* **108**, 10.1029/2002JD002670.

Rodwell M. J. and B. J. Hoskins, 2001. Subtropical anticyclones and summer monsoons. *J. Climate* **14**, 3192-3211.

Ropelewski C. F. and M. S. Halpert, 1986. North American precipitation and temperate patterns associated with the El Niño/Southern Oscillation. *Mon. Wea. Rev.* **114**, 2352-2362.

Ropelewski C. F. and M. S. Halpert, 1987. Global and regional scale precipitation pattern associates with the El Niño/Southern Oscilation. *Mon. Wea. Rev.* **115**, 16106-1626.

Ropelewski C. F. and M. S. Halpert, 1996. Quantifying southern oscillation-precipitation relationships. *J. Climate* **9**, 1043-1049.

Ropelewski C. F. and M. S. Halpert, 1998. Precipitation patterns associated with the high index phase of the southern oscillation. *J. Climate* **2**, 268-284.

Schubert S. D., M. J. Suárez, P. J. Region, R. D. Koster and J. T. Bacmeiter, 2004a. Causes of long-term drought in the United States Great Plains. *J. Climate* **17**, 485-503.

Schubert S. D., M. J. Suárez, P. J. Region, R. D. Koster and J. T. Bacmeiter, 2004b. On the cause of the 1930s dust bowl. *Science* **303**, 1855-1859.

Seager R., N. Harnik, Y. Kushnir, W. Robinson and J. Miller, 2003a. Mechanisms of hemispherically symmetric climate variability. *J. Climate* **16**, 2960-2978.

Seager R., R. Murtugudde, N. Naik, A. Clement, N. Gordon and J. Miller, 2003b. Air-sea interaction and the seasonal cycle of the subtropical anticyclones. *J. Climate* **16**, 1948-1966.

Seager R., A. Karspeck, M. Cane, Y. Kushnir, A. Giannini, A. Kaplan, B. Kerman and J. Vélez, 2004. Prediction Pacific decadal variability. Earth Climate. In: *The ocean-atmosphere interaction*. (C. Wang, X.-P. Xie and J. A. Carton, Eds.). American Geophysical Union, Washington DC, 115-130.

Seager R. N. Harnik, W. A. Robinson, Y. Kushnir. M. Ting, H. P. Huang and J. Vélez, 2005a. Mechanisms of ENSO-forcing of hemispherically symmetric precipitation variability. *Quart. J. Roy. Meteor. Soc*. **131**, 1501-1527.

Seager R., Y. Kushnir, C. Herweijer, N, Naik and J. Vélez, 1005b. Modelling of tropical forcing of persistent droughts and pluvials over western North America: 1856-2000. *J. Climate* **18**, 4068-4091.

Seager R., 2007. The turn-of-the-century North American drought: dynamics, global context and prior analogues. *J. Climate* **20**, 5527-5552.

Seager R., N. Graham, C. Herweijer, A. Gordon, Y. Kushnir and E. R. Cook, 2007a. Blueprints for medieval hydroclimate. *Quat. Sci. Rev.* **26**, 2322-2336.

Seager R., M. Ting, I. M. Held, Y. Kushnir, J. Lu, G. Vecchi, H. Huang, N. Harnik, A. Leetmaa, N. Lau, C. Li, J. Vélez and N. Naik, 2007b. Model projections of an imminent transition to a more arid climate in southwestern North America. *Science* **216**, 1881-1184.

Seager R., R. Burgman, Y. Kushnir, A. C. Clement, E. R. Cook, N. Naik and J. Vélez, 2008a. Tropical Pacific forcing of north american medieval megadroughts: Testing the concept with an atmosphere model forced by coral-reconstructed SSTs. *J. Climate.* In press.

Seager R., Y. Kushnir, M. Ting. M. A. Cane, N. Naik and J. Vélez, 2008b. Would advance knowledge of 1930s SSTs have allowed prediction of the Dust Bowl drought? *J. Climate* **21**, 3261-3281.

Stahle D. W. and M. K. Cleaveland, 1988. Texas drought history reconstructed and analyzed from 1698 to 1980. *J. Climate* **1**, 59-74.

Stahle D. W., E. R. Cook, M. K. Cleaveland, M. D. Therrel, D. Meko, H. Grissino-Mayer, E. Watson, and B. H. Luckman, 2000. Tree ring data document 16th century megadrought over North America. *Earth Observing System* (EOS), **18**, 121.

Stahle D. W., F. K. Fye, E. R. Cook and R. D. Griffin, 2007. Tree ring reconstructed megadroughts over North America since AD 1300. *Clim. Change* **83**, 133-149.

Ting M. and L. Yu, 1998. Steady response to tropical heating in wavy linear and nonlinear baroclinic models. *J. Atmos. Sci.* **55**, 3565-3582.

Trenberth K. and J. W. Hurrel, 1994. Decadal atmosphere-ocean variation in the Pacific. *Clim. Dyn*. **9**, 33-319.

Trenberth K., G. W. Branstator, D. Karoly, A. Kumar, N. Lau and C. Ropelewski, 1998. Progress during TOGA in understanding and modeling global teleconnections associated with tropical sea surface temperate. *J. Geophys. Res.* **103**, 14291-14324.

United States Department of Agriculture, Foreign Agriculture Service, 2006. México, NAFTA and Agriculture, a Snapshot. Technical Report GAIN Report number MX6060, United States Department of Agriculture, Foreign Agriculture Service, México City, 37 pp.

Villanueva-Díaz J., D. W. Stahle, B. Luckman, J. Cerano-Paredes, M. D. Therrell, M. K. Cleaveland and E. Cornejo-Oviedo, 2007. Winter-spring precipitation reconstructions from tree rings for northeast México. *Clim. Change* **83**, 117-131.

Wilder M. and P. R. Lankao, 2006. Paradoxes of decentralization: Water reform and social implications in México. *World Development* **34**, 1977-1995.